A molybdenum carbide catalyst with exceptional activity, selectivity, and stability for CO₂ conversion via high-temperature reverse water-gas shift

Milad Ahmadi Khoshooei^{1,2}*, Xijun Wang³, Gerardo Vitale², Filip Formalik^{3,4}, Kent O. Kirlikovali¹, Randall Q. Snurr³, Pedro Pereira-Almao², Omar K. Farha^{1,3}*

¹Department of Chemistry and International Institute for Nanotechnology, Northwestern University; Evanston, IL, 60208, United States.

²Department of Chemical and Petroleum Engineering, University of Calgary; Calgary, AB, T2N 1N4, Canada.

³Department of Chemical and Biological Engineering, Northwestern University; Evanston, IL, 60208, United States.

⁴Department of Micro, Nano and Bioprocess Engineering, Faculty of Chemistry, Wroclaw University of Science and Technology, Wroclaw, 50-370, Poland.

*Corresponding authors. Email: milad.ahmadikhoshooei@northwestern.edu (M.A.K.), o-farha@northwestern.edu (O.K.F.)

Abstract: Though technologically promising, the reduction of CO₂ to produce CO remains economically challenging due to the lack of an inexpensive, active, highly selective, and stable catalyst. We show that nanocrystalline cubic molybdenum carbide (α-Mo₂C), prepared via a facile and scalable route, offers 100% selectivity for CO₂ reduction to CO while maintaining its initial equilibrium conversion at high space velocity after over 500 h of exposure to harsh reaction conditions at 600 °C. The combination of operando and post-reaction characterization of the catalyst revealed that the high activity, selectivity, and stability are attributable to crystallographic phase purity, weak CO-Mo₂C interactions, and interstitial O atoms, respectively. Mechanistic studies and density functional theory (DFT) calculations provided evidence that the reaction proceeds via an H₂-aided redox mechanism.

One-Sentence Summary: A scalable catalyst for reducing CO₂ to CO at high temperatures is developed and promises the commercialization of an economical carbon conversion process.

Introduction

To address the ever-growing concentration of anthropogenic CO_2 in the atmosphere, governments and leaders worldwide have invested in developing efficient carbon capture technologies. As this technology develops, our global society should establish strategies to leverage captured CO₂ and potentially convert it into useful intermediates and chemicals. While sequestration and usage in enhanced oil recovery offer short-term solutions to handle the captured CO₂, carbon utilization appears to provide a long-term, more sustainable, economically circular, and geographyindependent pathway (1-3). In this context, global efforts towards developing a sustainable hydrogen network, known as blue and green hydrogen, have made the hydrogenation of CO₂ a promising CO₂ utilization pathway. Catalytic conversion of CO₂ is a multi-pronged effort (4) in which several end-products could be targeted depending upon a variety of influencing factors, including the availability of renewable energy and low carbon-intensity hydrogen, the possibility of development of tandem systems, the local market for the final product. In this context, production of CO via the reverse water-gas shift (RWGS) reaction is gaining attention since the produced CO or syngas (CO + H₂) can be used as building blocks to produce a variety of chemicals in tandem catalytic systems (5). Notably, most syngas conversion reactions are established commercial technologies, highlighting the immense value of CO and syngas. Economic studies show that CO-mediated CO₂ utilization routes could offer competitive benefits to other alternatives, particularly when access to renewable energy is readily available (6–10).

To realize the full potential of the RWGS reaction on this global scale, catalysts used must meet important criteria. First, techno-economic assessments of the RWGS reaction show that this process can only be overall carbon negative if the catalyst is 100% CO-selective so that no hydrogen is wasted towards the deleterious production of methane, which also simplifies the downstream separation process (11, 12). Additionally, the endothermic nature of the reaction necessitates relatively high operating temperatures (400-600 °C) and preferably high H₂:CO₂ ratios to obtain a sufficient one-pass conversion, which often results in sintering and agglomeration of the catalyst, especially in the case of multi-constituents Cu-based and noble metal-based catalysts (11, 13, 14). In this context, transition metal carbides, particularly molybdenum carbides, show promise as the components are earth-abundant and these materials can catalyze some chemical transformations with noble metal-like behavior. However, the synthesis of molybdenum carbide materials is either complex (15, 16) or requires noble metals to achieve certain active phases (17,

18). Moreover, controlling the crystallographic phase of the final product during synthesis while minimizing excessive carbon deposition necessitates using multi-step preparation processes or significant amounts of energy, precious precursors, and co-reagents, resulting in complex synthetic pathways that are difficult to scale up (19, 20). In the context of RWGS catalysts, single-constituent Mo-carbides suffer from unsatisfactory selectivity, poor stability under reaction conditions, loss of initial activity, or need additional constituents that may sinter upon exposure to high temperatures (fig. S1).

In this work, we report that a phase-pure cubic α-Mo₂C catalyst addresses these challenges and achieves 100% CO selectivity for the high-temperature RWGS reaction (at 300-600 °C, H₂:CO₂ = 0.5-4). Moreover, this catalyst demonstrates outstanding stability and maintains 100% of its initial activity and CO selectivity for at least 500 h under harsh conditions (600 °C, 0.1 MPag). It can be synthesized through a facile, inexpensive, and scalable route. Structural characterization studies after long-term stability tests confirm that the catalyst maintains its nanocrystalline domains that can explain its high activity, and a combination of mechanistic studies and density functional theory (DFT) calculations reveal that an H₂-assisted reduction of CO₂ governs the reaction mechanism. The catalyst offers high selectivity and stability over a wide range of temperatures, gas space velocities, and H₂:CO₂ ratios, enabling potential users to tailor the desired composition of the final product. More broadly, this catalyst may allow researchers to design tandem systems with absolute certainty and control of the first-stage products of an integrated approach, which is a significant challenge for RWGS catalysts (21). As this catalytic system converts CO₂ into CO in an effective, selective, and stable way while being able to accommodate different process conditions, this work overcomes limiting factors common to RWGS catalysts and produces an important C1 building block using an alternative, efficient route relative to those of conventional methods, which typically suffer from large carbon footprints due to the use of fossil fuels and high energy inputs.

Results and discussion Catalyst performance

To begin, we synthesized the phase-pure α -Mo₂C catalyst by carburizing (NH₄)₆Mo₇O₂₄·4H₂O and sucrose (household sugar), which serves as the carbon source, for 2 days at 500 °C under H₂, Fig. 1 (15). A comprehensive characterization of the catalyst is provided in the supplementary material.

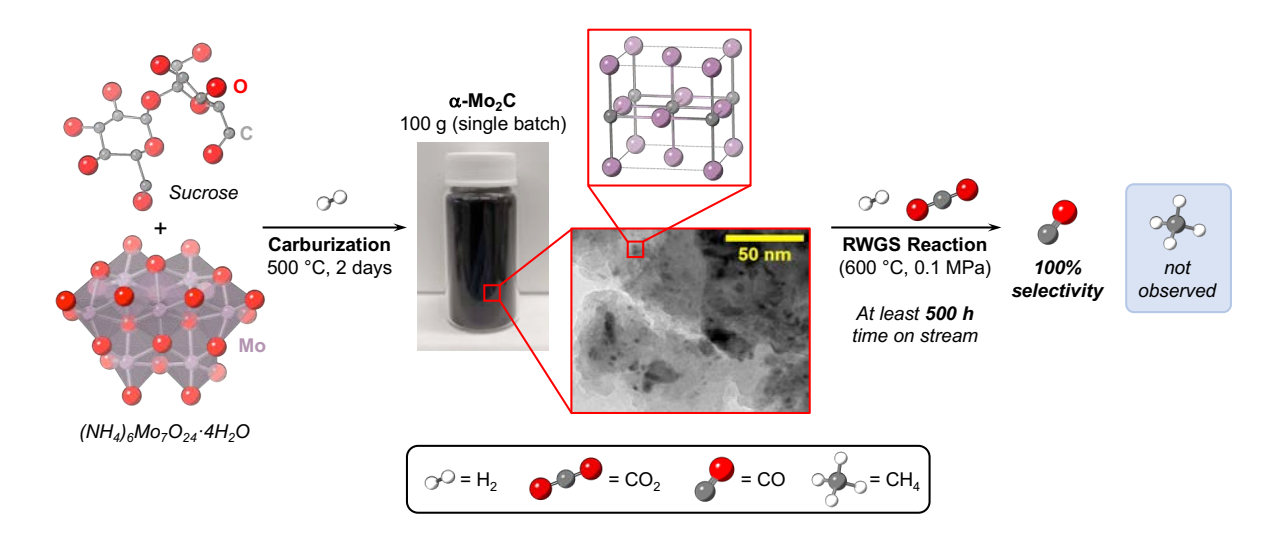


Fig. 1. Schematic of catalyst synthesis process and its performance for RWGS reaction.

We began by testing this catalyst across various temperature-space velocities and CO₂:H₂ ratios for the RWGS reaction. As shown in Fig. 2A, the catalyst shows near-equilibrium conversion at 500 °C under a high space velocity of 100,000 mL·g⁻¹·h⁻¹ and a CO₂:H₂ ratio of 3. Notably, over the entire temperature and CO₂:H₂ ratio ranges studied here, this catalyst is 100% CO-selective (Fig. 2, B and C), indicating that no methanation reaction occurs, even under favorable conditions for methanation reaction (e.g., a high CO₂:H₂ ratio of 1:4 and low temperatures of 300 °C). Gravimetric CO temperature programmed desorption (CO-TPD) data show that the CO desorption peak appears at ca. 120 °C (Fig. 2D), indicating that CO weakly adsorbs to the surface of the catalyst (22–24), confirming the inability of the catalyst to convert CO to methane and justifying the high selectivity of the catalyst. We further probed CO adsorption on the catalyst's surface using in-situ adsorption and desorption Fourier transform infrared (FT-IR) spectroscopic experiments. At sub-ambient temperatures, we observed a weak CO adsorption peak at 2018 cm⁻¹ on α-Mo₂C (25), which then disappeared upon heating the sample (desorption) at 100 °C, further highlighting the weak interaction of CO with the α-Mo₂C surface (fig. S2) (26). It is notable that this phase of Mo₂C shows better activity and selectivity relative to the hcp phase that is thermodynamically more stable under reaction conditions (fig S1). Additionally, the superior behavior of our catalyst over other α-Mo₂C catalysts can be attributed to metastability provided by the protecting carbonaceous layer and interstitial atoms (fig S1). The excess C:Mo atomic ratio employed in the synthesis, along with the available O atoms provided by sucrose, ensures that the phase-pure catalyst is synthesized in such a way that its durability is not compromised under the studied

reaction conditions. In comparison, other α -Mo₂C catalyst systems either rely on coordinating ligands, where their removal could potentially deteriorate RWGS catalytic performance (27), or lack the protecting carbonaceous layer to afford a loss of catalytic activity.

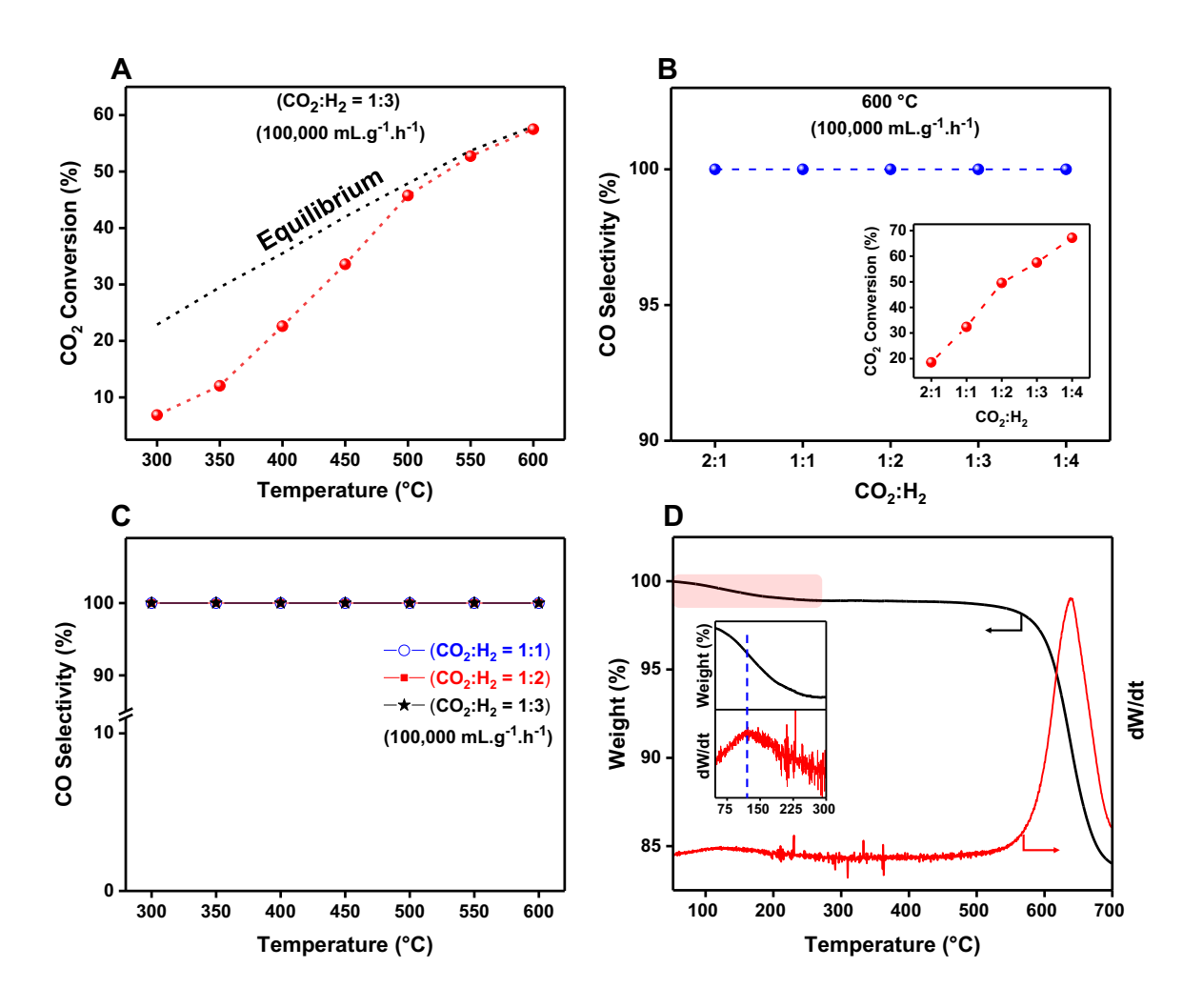


Fig. 2. Catalyst performance for reverse water gas shift reaction.

(A) CO₂ conversion at 100,000 mL.g⁻¹.h⁻¹ space velocity, 0.1 MPag, with CO₂:H₂ ratio of 1:3 in temperature range of 300-600 °C. (**B**) CO selectivity at 100,000 mL.g⁻¹.h⁻¹ at 600 °C in CO₂:H₂ ratio of 2:1 to 1:4. Inset: CO₂ conversion at 100,000 mL.g⁻¹.h⁻¹ space velocity, 0.1 MPag, at 600 °C with different CO₂:H₂ ratio in the range 2:1 to 1:4. (**C**) CO selectivity at 100,000 mL.g⁻¹.h⁻¹ space velocity, 0.1 MPag, with CO₂:H₂ ratio of 1:1 to 1:3 in temperature range of 300-600 °C. (**D**) Gravimetric CO temperature programmed desorption (TPD) study of in-situ activated catalyst (25 mg, Ar flow 40 sccm, 0.1 MPag, ramp rate 10 °C.min⁻¹). Inset: Mass change and first time-derivative of mass in the shaded temperature range 40-300 °C, showing a CO desorption peak at 120 °C.

Catalyst stability

This catalyst shows outstanding stability under harsh reaction conditions as it maintains both its initial activity and 100% CO-selectivity for at least 500-h on stream. We performed these experiments for systems operating at equilibrium (fig. S3), as well as away from equilibrium (Fig. 3A), to better highlight the stable nature of this catalyst and illustrate its potential application in industrially relevant equilibrium conversion. Powder X-ray diffraction (PXRD) analysis of the spent catalyst recovered following the long-term stability test reveals a slight shift in the diffraction peaks to the left, indicating an expansion in the unit cell by 0.1 Å (table S1), but shows no evidence of oxidation or crystallographic phase change of the catalyst and confirms the operational stability of this material (Fig. 3B). In comparison, the structurally reminiscent nanowire fcc α-MoC_{1-x} transforms to the hcp phase only after 20 h exposure to the same reactants at 600 °C (28). The increase in the unit cell parameter for α-Mo₂C may result from the removal of some of the interstitial atoms (O, N, or C) in the material (29) upon prolonged exposure to high temperatures, resulting in a change in the Mo-C bond length. Temperature-programmed desorption measurements conducted under an argon atmosphere ("Ar-TPD") from 100 to 850 °C show evidence for the removal of these atoms in the form of gaseous products (e.g., N₂ and CO₂) at temperatures beyond 600 °C (Fig. 3C). A similar observation is reported when Co, which is relatively smaller than Mo, is incorporated in the Mo₂C structure and results in both a unit cell contraction and a diffraction peak shift to higher angles (30). Both the fresh and spent catalysts feature crystallite sizes that are ca. 2 nm in size, which explains the catalyst's high activity after long exposure to the reactants, and comparisons between transmission electron microscopy (TEM) images of the fresh and spent catalysts do not reveal apparent changes in the material upon prolonged exposure to reactants under these harsh conditions (fig. S4). In addition, TEM images collected before and after catalysis illustrate the morphological uniformity of the catalyst, further highlighting that the protecting carbonaceous layer plays a pivotal role in providing stability to this catalyst. Combined, these observations confirm the excellent stability of this catalyst under the reaction conditions and suggest that its prolonged high activity may result from the lack of agglomeration or structural transformation during long exposure to the reaction conditions.

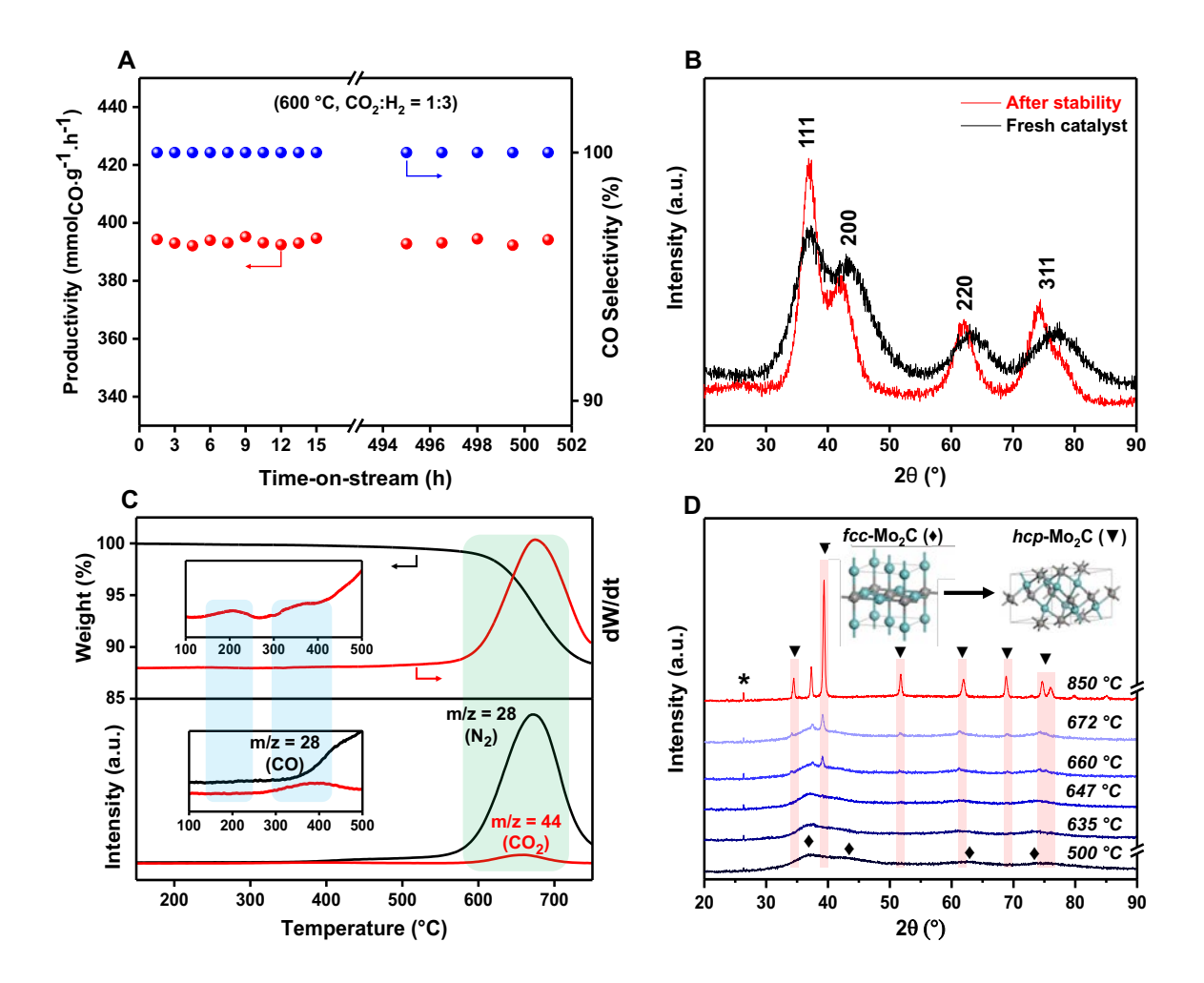


Fig. 3. Stability study of the catalyst under different conditions and environments.

(A) Long-term stability (> 500 h) of the α -Mo₂C catalyst for the RWGS reaction in the kinetic regime at 600,000 mL.g⁻¹.h⁻¹ space velocity, 0.1 MPag, with CO₂:H₂ ratio of 1:3 at 600 °C. (**B**) PXRD of the fresh (in-situ activated) and post-stability spent catalyst. (**C**) Gas evolution study of the in-situ activated catalyst under Ar environment as a function of temperature in the range 500-850 °C (ramp 1 °C.min⁻¹) in gravimetry (top), coupled with mass spectrometry (bottom) setup. Insets: Enlarged view of temperature range 100-500 °C. (**D**) In-situ PXRD study of the in-situ activated catalyst under H₂ environment as a function of temperature in the range 500-850 °C (ramp 1 °C.min⁻¹). The peak at 26° (*) is heat-induced and attributed to the carbonaceous part of the material.

Since gravimetric Ar-TPD experiments indicate considerable mass loss at temperatures beyond 600 °C, we next investigated the possible transformation of the catalyst upon high-temperature treatment under H₂ to better understand its long-term stability at 600 °C. We carried out in-situ PXRD measurements in which we slowly heated (1 °C·min⁻¹) the activated catalyst to 850 °C under an H₂ environment, revealing a gradual, irreversible phase transformation from the cubic

phase (fcc) to the hexagonal phase (hcp) that starts at 660-670 °C and corresponds to the highest rate of mass loss during the gravimetric Ar-TPD experiments (Fig. 3C). Notably, a peak at ca. 26° appears when heating the sample beyond 600 °C and corresponds to the heat-induced crystallization of the carbonaceous part of the material, and this peak disappears at temperatures below 600 °C while cooling the sample back to room temperature (fig S9). Similar phenomena have been reported in the literature for Mo-carbide materials containing carbonaceous counterparts (31), as well as generally for heat-induced crystallization processes in graphite-like carbonaceous materials (32, 33). In-situ calorimetry (fig. S5) shows a broad endothermic event with a peak at 670 °C, which is consistent with the in-situ PXRD and Ar-TPD results and likely results from the removal of interstitial atoms. Combined, these results suggest that the endothermic removal of a sufficient number of interstitial atoms perturbs the metastability of the cubic phase, and the material begins to transform into a more thermodynamically stable phase. Notably, the newly formed hexagonal close-packed (hcp) phase no longer shows 100% selectivity to CO at lower temperatures (table S2), which corroborates the selectivity previously observed for hexagonal Mo₂C catalysts (28) that are commonly produced via carburization of a Mo-containing precursor at relatively high temperatures (e.g., ≥ 800 °C) using CH₄ as the carbon source.

We then investigated the importance of each of the reactants (e.g., H_2 or CO_2) on catalytic performance. First, ex-situ PXRD experiments reveal that removal of either of the reactants at 600 °C results in either phase transformation (under H_2) or partial oxidation (under CO_2) only after 24 h of time-on-stream (fig. S7). In addition, ex-situ Raman spectroscopic studies also show that although H_2 treatment does not change the Raman fingerprint of the catalyst, CO_2 oxidizes the bulk of material to some extent (fig. S8). We further studied the *fcc* to *hcp* phase transformation using in-situ PXRD experiments and observed that under an H_2 environment at 600 °C, the phase transformation commences after only two hours of treatment (fig. S9). These results suggest the that long-term stability of α -Mo₂C under CO_2 hydrogenation conditions results from a kinetically governed phenomenon that prohibits a phase transformation and partial oxidation, both of which are unfavorable for activity and selectivity of the catalyst. A previous study shows that a similar phase transformation occurs for this material following treatment under H_2 at 500 °C for 15 h (29), and the longer transformation time likely results from the relatively lower available thermal energy at 500 °C for removal of the interstitial atoms.

Treatment of α-Mo₂C under H₂ at 600 °C for 24 h not only results in a phase transformation for the catalyst but also an increase in the average crystallite size by one order of magnitude to ca. 19 nm (table S2). In contrast, treatment of the fresh catalyst under CO₂, which partially oxidizes the bulk material, but with otherwise analogous conditions does not afford a significant change in the crystallite size, and the produced MoO₂ phases exhibit similar crystallite sizes (table S2). This phenomenon can potentially be attributed to the incorporation of O into the α-Mo₂C structure that oxidizes part of the carbidic structure. However, for the treatment under H₂, excessive removal of interstitial atoms perturbs the metastability of the cubic phase, and the material restructures into the more thermodynamically stable hcp phase. Yet, when both H₂ and CO₂ are present in the reaction mixture, the deleterious results observed upon exposure of α-Mo₂C to each individual gas do not occur, and therefore, the catalyst remains extraordinarily durable under the RWGS reaction conditions. This was further confirmed by carrying out in-situ PXRD experiments under different CO₂:H₂ ratios at 600 °C for 24 h, and we did not observe an adverse phase change in any of these cases (fig S7). It is important to note that the systematic removal either of the reactant was done to shed light on the stability of the catalyst, and thus, no operational risk is associated with this catalyst.

Reaction Mechanism

The RWGS reaction generally follows one of two pathways of redox mechanism or associative mechanism, where the difference is that, in the latter, the dissociated H species are involved in the formation of carbon-containing intermediates such as formate (HCOO*) or carboxylate (COOH*) (34). To probe the reaction mechanism, we first employed diffuse reflectance Fourier transform spectroscopy (DRIFTS) and studied the catalyst in-operando under the RWGS reaction conditions. Upon increasing the temperature from 300 to 500 °C under CO₂:H₂ of 1:3, we observed the emergence of peaks at 2111 cm⁻¹ and 2177 cm⁻¹ that are diagnostic for gaseous CO (fig. S10), as well as an increase in intensity for the peaks in the range 1400-1600 cm⁻¹ that potentially correspond to the appearance of reaction intermediates (Fig. 4B). Switching to ¹³CO₂ did not afford any noticeable shift in any of the peaks in the range 1400-1600 cm⁻¹ relative to those in the spectrum obtained under ¹²CO₂ (Fig. 4C), which suggests that these peaks are not kinetically relevant for the surface reaction on this catalyst under these reaction conditions and likely do not correspond to reaction intermediates. Notably, this observation contrasts conclusions drawn in studies using other Mo₂C catalysts that assign some of these peaks (e.g., 1386 cm⁻¹, 1511 cm⁻¹ (35),

or 1419 cm⁻¹ (28)) to formate species. Based on these in-situ DRIFTS results, peaks from 1400-1600 cm⁻¹ might be assigned to the vibrational fingerprint of species within the carbonaceous part of the material that arises from high temperatures or due to interactions with the guest molecules. Combined, these results rule out the associative mechanism that features a carbon-containing species as an intermediate, and thus, lead to us to infer that the RWGS reaction catalyzed by α -Mo₂C most likely proceeds through an H₂-assisted reduction of CO₂. Further discussion to support this idea is elaborated in the following sections.

Next, we carried out a comprehensive density functional theory (DFT) study of the catalyst and attempted to best match the experimentally observed O-modified α -Mo₂C structure, which we inferred from XPS data (fig. S6), as the pristine α-Mo₂C experiences a significant, irreversible surface reconstruction that makes the computational study of the reaction mechanism unrealistic (further discussions provided in Supplementary Materials). DFT calculations reveal that while the adsorption of CO₂ and H₂ are both energetically favorable, CO₂ adsorbs more favourably (Fig. 4A). Additionally, from the kinetic studies, we observed a lower reaction order for CO₂ relative to H₂ (fig. S11), confirming that the rate of reaction depends less on the surface concentration of CO₂ than that of H₂ (36). While H₂ dissociation has a negligible electronic energy barrier (confirming that dissociative adsorption of H₂ readily occurs under reaction conditions, see Supplementary Materials for further discussion), the dissociation of CO₂ into CO* and O* faces a free energy barrier of 0.73 eV, Fig. 4A. Further, DFT calculations show that the redox mechanism is energetically more favorable than HCOO*- or COOH*-mediated mechanisms (Fig. 4A and table S3), in agreement with the DRIFTS studies that the reaction most probably proceeds through the direct reduction pathway. Moreover, the CO desorption free energy is reasonably low under reaction conditions, further supporting the catalyst's selectivity for CO (Fig. 4A). In contrast, the direct reaction between OH* and H* presents a relatively formidable free energy barrier of 1.81 eV, whereas the reaction between two OH* species proves to be more feasible with a free energy barrier of 1.46 eV. Once H₂O* forms, the final step of water desorption occurs freely under reaction temperature. It is also noteworthy that water formation is the step with the highest free energy barrier, which is consistent with the observed inverse kinetic isotopic effect (fig. S12). The DFT results are in good agreement with previously reported results for the hcp-Mo₂C system (37).

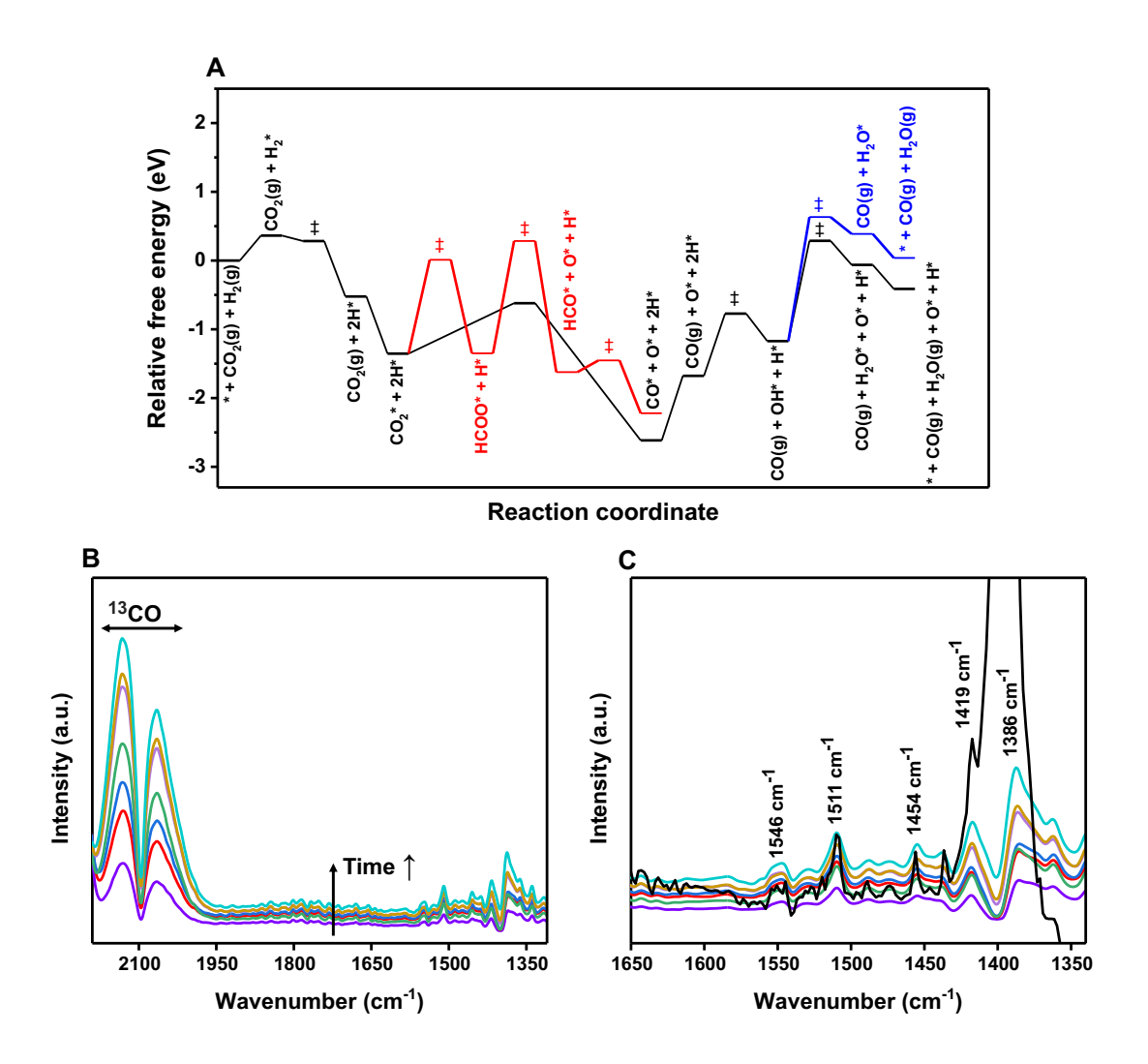


Fig. 4. Investigation of the reaction mechanism.

(A) Computed free energy profiles of the redox and formate-mediated (HCOO*) mechanisms for the RWGS reaction on O-modified α -Mo₂C(001) surface at 500 °C. Black and red are attributed to the redox and formate-mediated pathways, respectively. Blue indicates the formation of H₂O from the reaction between OH* and H* species. (**B** and **C**) Operando DRIFTS study of the RWGS at 0.1 MPag and CO₂:H₂ of 1:3 on the in-situ activated catalyst, for exploring reaction mechanism using 13 CO₂ + H₂ (**B**) in a recirculating mode at 500 °C as a function of time and (**C**) Enlarged view of lower wavenumber region in (B), black line shows 12 CO₂ + H₂ corresponding spectrum for comparison.

Next, we shifted our focus on decoupling the half-reactions happening on the surface of the catalyst, presumably: $CO_2+Mo_xC_y \rightarrow CO + Mo_xC_yO$ and $Mo_xC_yO + H_2 \rightarrow Mo_xC_y + H_2O$. First, we flowed CO_2 over the activated catalyst in an in-situ DRIFTS setup and observed the production and subsequent dissipation of CO (Fig. 5, A to E), 2115-2120 cm⁻¹ and 2170-2180 cm⁻¹ (with a node at 2143 cm⁻¹) which suggests the dissociation of CO_2 to CO(g) and O^* species over this

period. While CO desorbs from the surface, the O atom likely integrates into the α-Mo₂C structure to form an oxycarbide species (*38*) as CO₂ has been shown to passivate metal carbide materials by forming an oxycarbide layer on the surface, preventing their bulk oxidation (*39*). Next, the reduction step proceeds upon switching the flow to H₂, and the gaseous CO peaks become sharper due to the RWGS reaction with a high H₂/CO₂ ratio (Fig. 5, F to J). Notably, gaseous CO peaks dissipate upon further H₂ exposure as CO₂ is consumed, which we confirmed in a recirculating system with ¹³CO₂ (fig. S10), and reappear upon re-exposure to CO₂ (fig. S13). Again, these result suggest that the direct reduction of CO₂ could be the reaction pathway.

We then performed an in-situ thermogravimetric/calorimetric (TG-DSC) study in which we alternated the environment between CO₂ and H₂ at 400 °C and measured both the mass changes and the heat flow from the reaction (Fig. 5K). Initially, the freshly activated catalyst shows considerable mass gain upon exposure to CO₂ (ca. 0.5 wt%), which corroborates results from similar studies (38, 40, 41), and corresponds to an exothermic peak of 91 kJ·mol⁻¹ on the calorimetric diagram. After switching the environment to H₂, we observe a mass loss of ca. 0.15 wt % and a corresponding endothermic peak in the thermogravimetric and calorimetric data, respectively, which is consistent with the endothermic nature of the RWGS reaction. The magnitude of mass loss during this H₂ step is smaller than the mass gained during the initial CO₂ step (i.e., the initial mass gain is not fully recoverable under H₂), suggesting that CO₂ reacts with the surface of the catalyst under the reaction conditions and presumably forms an oxycarbide species, which is consistent with the conclusions drawn from flow DRIFTS, Raman (fig. S7), and PXRD (fig. S8) experiments described above, as well as results from similar studies (40). In addition, the second and third CO₂ adsorption cycles afford higher exothermic enthalpies of 112 and 114 kJ·mol⁻¹, respectively, relative to that of the first CO₂ adsorption cycle, indicating that the first cycle features other enthalpic and mass gain contributions that combine to afford a lower enthalpy per unit mole of adsorbed CO₂ (i.e., formation of oxycarbide species upon the reaction between CO₂ and the α-Mo₂C surface (42)). After the first cycle, the cyclic mass gain, mass loss, and switch of enthalpic events become consistent, providing further evidence for the formation of an oxycarbide species during the first cycle.

To rule out the possibility that CO could form, when only CO_2 is present, through the reverse Boudouard reaction, we exposed the α -Mo₂C at 500 °C to $^{13}CO_2$ (fig. S14) in a recirculating setup at 0.1 MPag. Consumption of $^{13}CO_2$ in a recirculating mode generates only ^{13}CO (no fingerprint

of ¹²CO is observed), confirming that the reduction of CO₂ on the catalyst via the RWGS reaction is the sole reason for CO production. We then further explored the H₂-dependency of the reaction by observing that the apparent activation energy of the reaction depends on the H₂/CO₂ ratio, where higher ratios of H₂ to CO₂ facilitate the reduction of CO₂ to CO (fig. S11). Differential thermogravimetry studies (Fig. 5L) also show that the step involving CO₂ activation is faster than that of H₂ activation and subsequent CO₂ reduction via the RWGS (per mass basis of the two lumped half-reactions), which corroborates the kinetic data and the observed inverse kinetic isotopic effects (fig. S12).

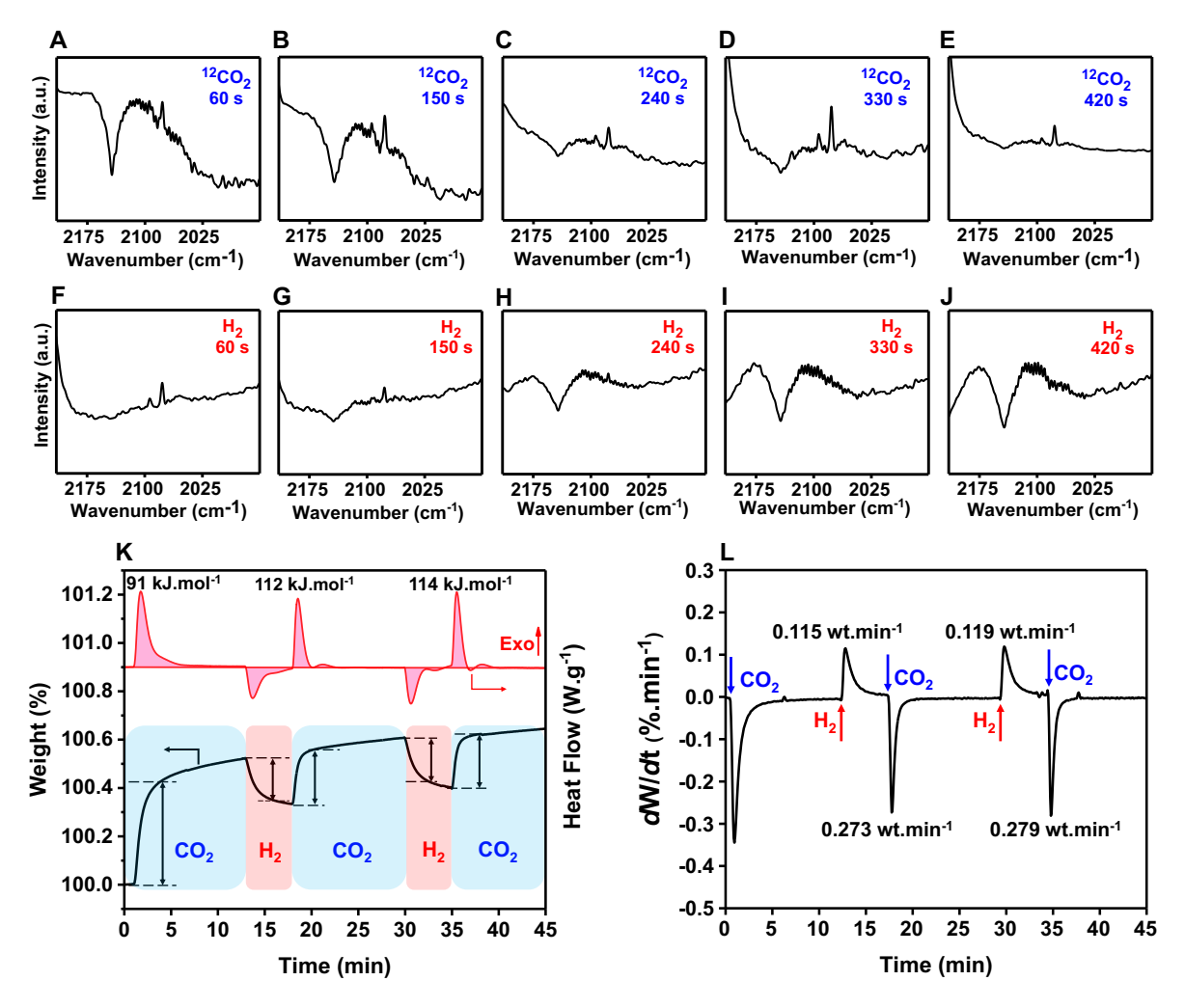


Fig. 5. Decoupling of half-reactions in redox mechanism.

(**A-J**) Operando DRIFTS study of the RWGS at 0.1 MPag on in-situ activated catalyst at 500 °C, under ¹²CO₂ environment, peaks at 2117 cm⁻¹ and 2177 cm⁻¹ along with the node at 2143 cm⁻¹ corresponds to ¹²CO. (**A-E**) and subsequent switch of the environment to H₂ (**F-J**) as a function of time. (**K** and **L**) In-situ thermogravimetry/calorimetry (K) and differential thermogravimetry (L)

studies of the RWGS at 0.1 MPag on the in-situ activated catalyst (25 mg) at 400 °C under subsequent environmental switch between CO_2 and H_2 , 100 sccm 10% CO_2/N_2 and 100 sccm 10% H_2/N_2 (The mass gains and losses in (K) identified by dashed lines are obtained from the second time derivative of mass profile (fig. S14), where the rate of mass change becomes constant with respect to time, i.e. second derivative of mass becomes zero).

Outlook

Developing a reverse water gas shift (RWGS) process that operates at ambient pressure would require low capital cost infrastructure to convert CO₂ to CO. Moreover, leveraging electrical energy to heat endothermic reactions can further reduce the carbon footprint of CO₂ conversion processes (43, 44), such as the RWGS reaction. In addition, process intensification of the RWGS can further enhance its efficiency by pushing the conversion of this equilibrium-limited endothermic reaction (45). Moreover, due to its endothermic nature, the RWGS reaction becomes more carbon-negative at higher temperatures (10). Therefore, developing a stable and 100%-CO selective catalyst under industrially relevant process conditions is the current bottleneck for the industrialization of this process. Though stable catalysts for the RWGS have been reported for long-term operation at milder conditions (46), the α-Mo₂C catalyst reported in this work demonstrates the desired selectivity and stability, along with the flexibility in accommodating various operating parameters without loss of performance under high temperature conditions, and features a facile and low-cost synthesis procedure. As a result, α-Mo₂C could potentially offer a pathway for the successful commercialization of the RWGS process either to produce syngas (or CO) or as an intermediate step for producing value-added commodities from CO₂ and renewable hydrogen, ideally using renewable sources of energy or waste heat.

Acknowledgments

We acknowledge Prof. Justin M. Notestein for fruitful discussions. MAK is grateful for the Postdoctoral Fellowship provided by the Natural Sciences and Engineering Research Council of Canada (NSERC). This work made use of the Jerome B.Cohen X-Ray Diffraction Facility supported by the MRSEC program of the National Science Foundation (DMR-2308691) at the Materials Research Center of Northwestern University and the Soft and Hybrid Nanotechnology Experimental (SHyNE) Resource (NSF ECCS-2025633). This work made use of the Keck-II facility of Northwestern University's NUANCE Center, which has received support from the SHyNE Resource (NSF ECCS-2025633), the IIN, and Northwestern's MRSEC program (NSF

DMR-2308691). The REACT Facility of the Northwestern University Center for Catalysis and Surface Science is supported by a grant from the DOE (DE-SC0001329). The authors thank Dr. Selim Alayoglu for helping with the DRIFTS experiments. This research used resources of the National Energy Research Scientific Computing Center (NERSC); a DOE Office of Science User Facility supported by the Office of Science of the U.S. Department of Energy under contract no.DE-AC02-05CH11231 using NERSC award BES-ERCAP0023154. This research was also supported in part through the computational resources and staff contributions provided for the Quest high performance computing facility at Northwestern University which is jointly supported by the Office of the Provost, the Office for Research, and Northwestern University Information Technology.

Funding: This work was partly supported by the Catalyst Design for Decarbonization Center, an Energy Frontier Research Center, which is funded by the US Department of Energy (DOE), Office of Science, Basic Energy Sciences (BES) DE-SC0023383. RQS acknowledges support from the U.S. National Science Foundation (award no. 2119433).

Author contributions:

Initiation & Conceptualization: MAK

Methodology & Experiment Design: MAK

Investigation: MAK, XW, GV, FF

Funding acquisition: RQS, OKF

Project administration: MAK, OKF

Supervision: RQS, PPA, OKF

Writing – original draft: MAK, XW, KOK

Writing – review & editing: KOK, GV, RQS, PPA, OKF

Competing interests: The authors declare no competing interests.

Data and materials availability: All data and images are available in the manuscript or the supplementary materials.

Supplementary Materials:

Materials and Methods Supplementary Text Figs. S1 to S42 Tables S1 to S3 References (46-68)

References

- 1. N. Mac Dowell, P. S. Fennell, N. Shah, G. C. Maitland, The role of CO2 capture and utilization in mitigating climate change. *Nat Clim Chang* **7**, 243–249 (2017).
- 2. C. Hepburn, E. Adlen, J. Beddington, E. A. Carter, S. Fuss, N. Mac Dowell, J. C. Minx, P. Smith, C. K. Williams, The technological and economic prospects for CO2 utilization and removal. *Nature* **575**, 87–97 (2019).
- 3. A. Saravanan, P. Senthil kumar, D.-V. N. Vo, S. Jeevanantham, V. Bhuvaneswari, V. Anantha Narayanan, P. R. Yaashikaa, S. Swetha, B. Reshma, A comprehensive review on different approaches for CO2 utilization and conversion pathways. *Chem Eng Sci* **236**, 116515 (2021).
- 4. O. Martin, A. J. Martín, C. Mondelli, S. Mitchell, T. F. Segawa, R. Hauert, C. Drouilly, D. Curulla-Ferré, J. Pérez-Ramírez, Indium Oxide as a Superior Catalyst for Methanol Synthesis by CO2 Hydrogenation. *Angewandte Chemie International Edition* **55**, 6261–6265 (2016).
- 5. X. Gao, T. Atchimarungsri, Q. Ma, T.-S. Zhao, N. Tsubaki, Realizing efficient carbon dioxide hydrogenation to liquid hydrocarbons by tandem catalysis design. *EnergyChem* **2**, 100038 (2020).
- 6. B. Anicic, P. Trop, D. Goricanec, Comparison between two methods of methanol production from carbon dioxide. *Energy* **77**, 279–289 (2014).
- 7. O.-S. Joo, K.-D. Jung, I. Moon, A. Ya. Rozovskii, G. I. Lin, S.-H. Han, S.-J. Uhm, Carbon Dioxide Hydrogenation To Form Methanol via a Reverse-Water-Gas-Shift Reaction (the CAMERE Process). *Ind Eng Chem Res* **38**, 1808–1812 (1999).
- 8. O. G. Sánchez, Y. Y. Birdja, M. Bulut, J. Vaes, T. Breugelmans, D. Pant, Recent advances in industrial CO2 electroreduction. *Curr Opin Green Sustain Chem* **16**, 47–56 (2019).
- 9. K. Harris, R. G. Grim, Z. Huang, L. Tao, A comparative techno-economic analysis of renewable methanol synthesis from biomass and CO2: Opportunities and barriers to commercialization. *Appl Energy* **303**, 117637 (2021).
- 10. O. Y. H. Elsernagawy, A. Hoadley, J. Patel, T. Bhatelia, S. Lim, N. Haque, C. Li, Thermo-economic analysis of reverse water-gas shift process with different temperatures for green methanol production as a hydrogen carrier. *Journal of CO2 Utilization* **41**, 101280 (2020).

- 11. S. Roy, A. Cherevotan, S. C. Peter, Thermochemical CO2 Hydrogenation to Single Carbon Products: Scientific and Technological Challenges. *ACS Energy Lett* **3**, 1938–1966 (2018).
- 12. R. M. Bown, M. Joyce, Q. Zhang, T. R. Reina, M. S. Duyar, Identifying Commercial Opportunities for the Reverse Water Gas Shift Reaction. *Energy Technology* **9**, 2100554 (2021).
- 13. Y. A. Daza, J. N. Kuhn, CO2 conversion by reverse water gas shift catalysis: comparison of catalysts, mechanisms and their consequences for CO2 conversion to liquid fuels. *RSC Adv* **6**, 49675–49691 (2016).
- 14. M. D. Porosoff, B. Yan, J. G. Chen, Catalytic reduction of CO2 by H2 for synthesis of CO, methanol and hydrocarbons: challenges and opportunities. *Energy Environ Sci* **9**, 62–73 (2016).
- 15. M. Ahmadi Khoshooei, G. Vitale, L. Carbognani, P. Pereira-Almao, Evidence of water dissociation and hydrogenation on molybdenum carbide nanocatalyst for hydroprocessing reactions. *Catal Sci Technol*, doi: 10.1039/D2CY01341J (2022).
- L. R. Karadaghi, M. S. Madani, E. M. Williamson, A. T. To, S. E. Habas, F. G. Baddour, J. A. Schaidle, D. A. Ruddy, R. L. Brutchey, N. Malmstadt, Throughput Optimization of Molybdenum Carbide Nanoparticle Catalysts in a Continuous Flow Reactor Using Design of Experiments. ACS Appl Nano Mater 5, 1966–1975 (2022).
- 17. X. Sun, J. Yu, S. Cao, A. Zimina, B. B. Sarma, J.-D. Grunwaldt, H. Xu, S. Li, Y. Liu, J. Sun, In Situ Investigations on Structural Evolutions during the Facile Synthesis of Cubic α-MoC1–x Catalysts. *J Am Chem Soc*, doi: 10.1021/jacs.2c08979 (2022).
- 18. X. Sun, J. Yu, X. Tong, M. Yang, J. Zhang, J. Sun, Controlling phase transfer of molybdenum carbides by various metals for highly efficient hydrogen production. *Journal of Energy Chemistry* **62**, 191–197 (2021).
- 19. X. Du, R. Zhang, D. Li, C. Hu, H. Garcia, Molybdenum carbide as catalyst in biomass derivatives conversion. *Journal of Energy Chemistry* **73**, 68–87 (2022).
- 20. O. Rabi, E. Pervaiz, R. Zahra, M. Ali, M. B. K. Niazi, An inclusive review on the synthesis of molybdenum carbide and its hybrids as catalyst for electrochemical water splitting. *Molecular Catalysis* **494**, 111116 (2020).
- 21. R. Belgamwar, R. Verma, T. Das, S. Chakraborty, P. Sarawade, V. Polshettiwar, Defects Tune the Strong Metal–Support Interactions in Copper Supported on Defected Titanium Dioxide Catalysts for CO2 Reduction. *J Am Chem Soc* **145**, 8634–8646 (2023).

- 22. Z. Zhao, M. Wang, P. Ma, Y. Zheng, J. Chen, H. Li, X. Zhang, K. Zheng, Q. Kuang, Z.-X. Xie, Atomically dispersed Pt/CeO2 catalyst with superior CO selectivity in reverse water gas shift reaction. *Appl Catal B* **291**, 120101 (2021).
- 23. H. Wang, M. S. Bootharaju, J. H. Kim, Y. Wang, K. Wang, M. Zhao, R. Zhang, J. Xu, T. Hyeon, X. Wang, S. Song, H. Zhang, Synergistic Interactions of Neighboring Platinum and Iron Atoms Enhance Reverse Water–Gas Shift Reaction Performance. *J Am Chem Soc* **145**, 2264–2270 (2023).
- 24. H. Shen, Y. Dong, S. Yang, Y. He, Q. Wang, Y. Cao, W. Wang, T. Wang, Q. Zhang, H. Zhang, Identifying the roles of Ce3+-OH and Ce-H in the reverse water-gas shift reaction over highly active Ni-doped CeO2 catalyst. *Nano Res* **15**, 5831–5841 (2022).
- 25. W. Wu, Z. Wu, C. Liang, X. Chen, P. Ying, C. Li, In Situ FT-IR Spectroscopic Studies of CO Adsorption on Fresh Mo2C/Al2O3 Catalyst. *J Phys Chem B* **107**, 7088–7094 (2003).
- 26. E. Chukwu, L. Molina, C. Rapp, L. Morales, Z. Jin, S. Karakalos, H. Wang, S. Lee, M. J. Zachman, M. Yang, Crowded supported metal atoms on catalytically active supports may compromise intrinsic activity: A case study of dual-site Pt/α-MoC catalysts. *Appl Catal B* **329**, 122532 (2023).
- 27. F. G. Baddour, E. J. Roberts, A. T. To, L. Wang, S. E. Habas, D. A. Ruddy, N. M. Bedford, J. Wright, C. P. Nash, J. A. Schaidle, R. L. Brutchey, N. Malmstadt, An Exceptionally Mild and Scalable Solution-Phase Synthesis of Molybdenum Carbide Nanoparticles for Thermocatalytic CO2 Hydrogenation. *J Am Chem Soc* 142, 1010–1019 (2020).
- 28. J. Gao, Y. Wu, C. Jia, Z. Zhong, F. Gao, Y. Yang, B. Liu, Controllable synthesis of α-MoC1-x and β-Mo2C nanowires for highly selective CO2 reduction to CO. *Catal Commun* **84**, 147–150 (2016).
- 29. K. O. Sebakhy, G. Vitale, A. Hassan, P. Pereira-Almao, New Insights into the Kinetics of Structural Transformation and Hydrogenation Activity of Nano-crystalline Molybdenum Carbide. *Catal Letters* **148**, 904–923 (2018).
- 30. T.-C. Xiao, A. P. E. York, H. Al-Megren, C. V Williams, H.-T. Wang, M. L. H. Green, Preparation and Characterisation of Bimetallic Cobalt and Molybdenum Carbides. *J Catal* **202**, 100–109 (2001).
- 31. B. Deng, Z. Wang, W. Chen, J. T. Li, D. X. Luong, R. A. Carter, G. Gao, B. I. Yakobson, Y. Zhao, J. M. Tour, Phase controlled synthesis of transition metal carbide nanocrystals by ultrafast flash Joule heating. *Nat Commun* **13**, 262 (2022).

- 32. T. Qiu, J. Yang, X. Bai, Insight into the change in carbon structure and thermodynamics during anthracite transformation into graphite. *International Journal of Minerals, Metallurgy and Materials* **27**, 162–172 (2020).
- 33. Z. Chen, Y. Gu, L. Hu, W. Xiao, X. Mao, H. Zhu, D. Wang, Synthesis of nanostructured graphite via molten salt reduction of CO2 and SO2 at a relatively low temperature. *J Mater Chem A Mater* **5**, 20603–20607 (2017).
- 34. X. Su, X. Yang, B. Zhao, Y. Huang, Designing of highly selective and high-temperature endurable RWGS heterogeneous catalysts: recent advances and the future directions. *Journal of Energy Chemistry* **26**, 854–867 (2017).
- 35. J. Xu, X. Gong, R. Hu, Z. Liu, Z. Liu, Highly active K-promoted Cu/β-Mo2C catalysts for reverse water gas shift reaction: Effect of potassium. *Molecular Catalysis* **516**, 111954 (2021).
- 36. H.-X. Liu, S.-Q. Li, W.-W. Wang, W.-Z. Yu, W.-J. Zhang, C. Ma, C.-J. Jia, Partially sintered copper—ceria as excellent catalyst for the high-temperature reverse water gas shift reaction. *Nat Commun* 13, 867 (2022).
- 37. H. Jing, Q. Li, J. Wang, D. Liu, K. Wu, Theoretical Study of the Reverse Water Gas Shift Reaction on Copper Modified β-Mo2C(001) Surfaces. *The Journal of Physical Chemistry C* **123**, 1235–1251 (2019).
- 38. F. Solymosi, A. Oszkó, T. Bánsági, P. Tolmacsov, Adsorption and Reaction of CO2 on Mo2C Catalyst. *J Phys Chem B* **106**, 9613–9618 (2002).
- 39. L. Lin, W. Sheng, S. Yao, D. Ma, J. G. Chen, Pt/Mo2C/C-cp as a highly active and stable catalyst for ethanol electrooxidation. *J Power Sources* **345**, 182–189 (2017).
- 40. H. Zhou, Z. Chen, E. Kountoupi, A. Tsoukalou, P. M. Abdala, P. Florian, A. Fedorov, C. R. Müller, Two-dimensional molybdenum carbide 2D-Mo2C as a superior catalyst for CO2 hydrogenation. *Nat Commun* **12**, 5510 (2021).
- 41. M. D. Porosoff, X. Yang, J. A. Boscoboinik, J. G. Chen, Molybdenum Carbide as Alternative Catalysts to Precious Metals for Highly Selective Reduction of CO2 to CO. *Angewandte Chemie International Edition* **53**, 6705–6709 (2014).
- 42. A. R. S. Darujati, D. C. LaMont, W. J. Thomson, Oxidation stability of Mo2C catalysts under fuel reforming conditions. *Appl Catal A Gen* **253**, 397–407 (2003).
- 43. K. Yu, C. Wang, W. Zheng, D. G. Vlachos, Dynamic Electrification of Dry Reforming of Methane with In Situ Catalyst Regeneration. *ACS Energy Lett* **8**, 1050–1057 (2023).

- 44. L. Zheng, M. Ambrosetti, A. Beretta, G. Groppi, E. Tronconi, Electrified CO2 valorization driven by direct Joule heating of catalytic cellular substrates. *Chemical Engineering Journal* **466**, 143154 (2023).
- 45. D. Esposito, Pulling H2O out. *Nat Catal* **6**, 290 (2023).
- 46. G. Kim, S. H. Ryu, H. Jeong, Y. Choi, S. Lee, J. H. Choi, H. Lee, Easily Scalable Shell-Structured Copper Catalyst with High Activity and Durability for Carbon Dioxide Hydrogenation. *Angewandte Chemie International Edition*, e202306017 (2023).